Spatial Correlation of Tuberculosis (TB) Incidents to the MODIS LST Biophysical Signature of African Countries

Andreas Tsatsaris[#1], George Miliaresis[#2]

Department of Surveying Engineering, Technological Educational Institute of Athens
Ag. Spiridonos & Pallikaridi St., Egaleo, Athens, Greece.
Remote Sensing & GIS Center, Sultan Qaboos University,
P.O. Box 33, Al-Khod PC 123, Sultanate of Oman
[1]atsats@teiath.gr
[2]miliaresis.g@gmail.com

***Abstract*- Monthly night averaged land surface temperature (LST) imagery is analyzed throughout a year-period (2008), in an attempt to capture the seasonal variability of LST, and parametrically represent and classify the African Countries. Segmentation outlined in an objective way the temporal variation of LST during the 2008, grouped in 9 zones with distinct spatial distribution, each one presenting a distinct annual variation of monthly LST. Tuberculosis incidence per county for the year 2008 was correlated to the percentage areal occurrence of the 9 biophysical zones. More specifically statistical analysis indicates that there is an increase of TB-IR per country if the percent occurrence of either zone 4 or zone 6 is increased. Such evidence was already known, but it is the first time that this correlation was quantified on the basis of high resolution LST data comparable to the previous studies that were based on the very sparse meteorological stations network. The MODIS multi-temporal LST data can assist the modeling of the disease risk and disease spatial distribution as well as environmental modeling, climatic change studies at moderate resolution/country level scale.**

***Keywords*- Tuberculosis; environmental health; geographical information systems; land surface temperature; MODIS**

I. INTRODUCTION

Biophysical data includes land cover [1], land surface temperature (LST) [2], sea surface temperature, tree canopy density [3], [4], etc. These parameters are of great importance in assessing environmental change [5]. The modern operational space-borne sensors with spectral sensitivity in the thermal infra-red spectrum allow monitoring of the Earth's thermal field at a moderate spatial resolution [6]. Thus, thermal imagery products are available on regular and frequent basis for both the land and the oceans. Data availability stimulates the analysis of the long time series of thermal images in an attempt to closely monitor regions and provide information about the changes in LST from multi-temporal imagery [7], [8], [9].

Climate change, elevation and land cover are environmental factors that are strongly related to the spread of specific infectious diseases which have emerged or re-emerged in the last years in many countries all over the world [10]. It might be proved precious to the modelling of the spatial distribution of infectious diseases, if the biophysical parameters, such as LST, are included in the modeling processing chain.

Since 1975, the World Health Organization reports, over 30 diseases have appeared that are new to medicine included are AIDS, Ebola, Lyme disease, Legionnaires' disease, toxic Escherichia coli, a new hantavirus, and a rash of rapidly evolving antibiotic-resistant organisms, while of equal concern is the resurgence of old diseases, such as malaria and cholera [11]. Declines in social conditions and public health programs underlie the rebound of diseases transmitted person-to-person (e.g., tuberculosis (TB), diphtheria). It has been found that seasonal variation of temperature is correlated to the geographical distribution of TB [12], [13], especially in countries and continents where the climate variation has result the increase of the vulnerability of the disease.

The Africa Continent (which is a very good paradigm of climate variation), extents in both the Northern and Eastern Hemisphere and includes many countries with diverse environment, land cover and biophysical conditions [14]. The quantification of knowledge related to the Africa as well as to the distinct countries included in the Continent is a key factor in an attempt to characterize the landscape, to assess the sensitivity to natural hazards and to support environmental

analysis and diseases risk studies at moderate resolution scale.

Since temperature plays a key role to the spatial distribution of certain diseases while the modern biophysical imagery [15] provides LST data with increased both spatial and temporal resolution comparable to the sparse meteorological network coverage, our aim is to include LST data to the parametric representation of African Countries and correlate the derived parametric representation to incidents per disease per country [16].

Towards this end, monthly night averaged LST imagery will be analyzed throughout a year-period (2008), in an attempt to capture the seasonal variability of LST, segment the Africa Continent to climatic zones with different LST annual variability, and parametrically represent the African countries on the basis of the percent occurrence of the derived climatic zones. Finally, the LST parametric representation per country will be correlated to the number of incidents per 100,000 inhabitants for TB, a disease with severe impact to African population and economy.

The disease data are provided on a country level [16] and thus, the biophysical data should be also expressed at a country level for statistical evaluations to be feasible.

II. Methodology

Firstly, the study area, the spatial objects (the countries of Africa), the LST multi-temporal imagery and the TB incidents per country are presented. Then, the terrain is segmented to regions from the multi-temporal LST data, each region presenting a different climatic zone and these zones are used in spatial objects parametric representation and classification. Finally, the percent occurrence of the derived climatic zones per country is correlated to the number of incidents per 100,000 inhabitants.

A. Study area and the spatial objects

The study area corresponds to Africa Continent bounded by latitudes -36^o South to 38^o North and longitudes -18^o West to 52^o East. 49 countries (spatial objects) are included within this region (Fig. 1). Note that only the countries with significant area extent were included in this study [17]. Small islands (with area extent less than 3 times the pixel size of the satellite imagery used) that form independent states were omitted.

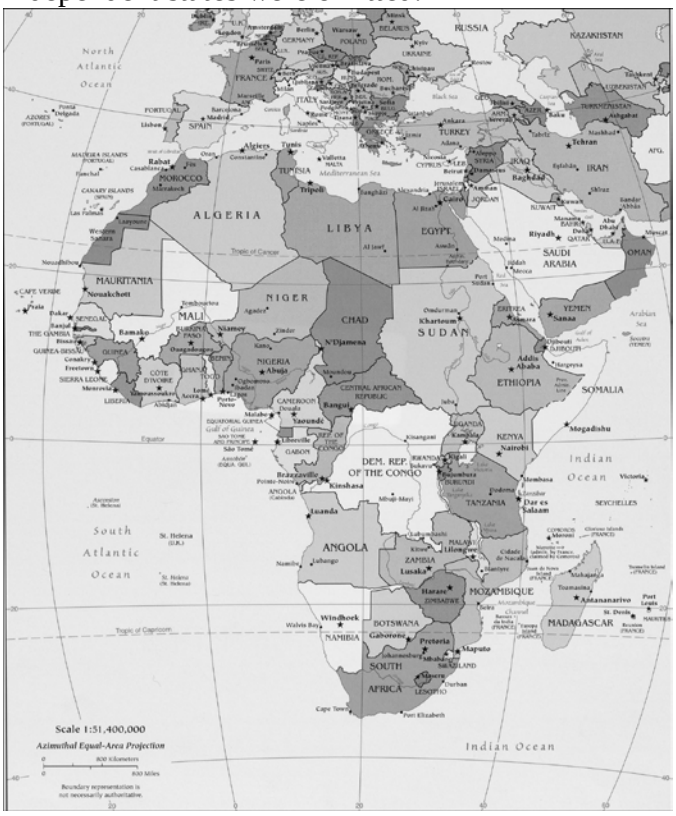


Fig. 1. The border of the major Countries (49 objects with the greatest area extent) of Africa (African Maps 2010).

B. Multi-temporal LST Data

The LST dataset (with accuracy 1 Kelvin) derived from MODerate-resolution Imaging Spectroradiometer (MODIS) instrument on board the Terra polar orbiting satellite was used [6]. These products are available on regular and frequent basis for both the land and the oceans. Note that morning (10:30AM) and late evening (10:30PM) passes are available daily from the Terra satellite.

Monthly averaged data for both the ascending pass (daytime) and descending pass (night time) are available from 2001 to date [15]. More specifically, the days and nights in clear-sky conditions and with validated LST values within a calendar month are composited and averaged. Thus, images correspond to mean monthly LST values on 0.05 degree latitude/longitude grid (forming 5.6 km * 5.6 km grid at the equator) referenced to WGS84 ellipsoid. The 12 images that correspond to the monthly night LST of the year 2008 were used (Fig. 2).

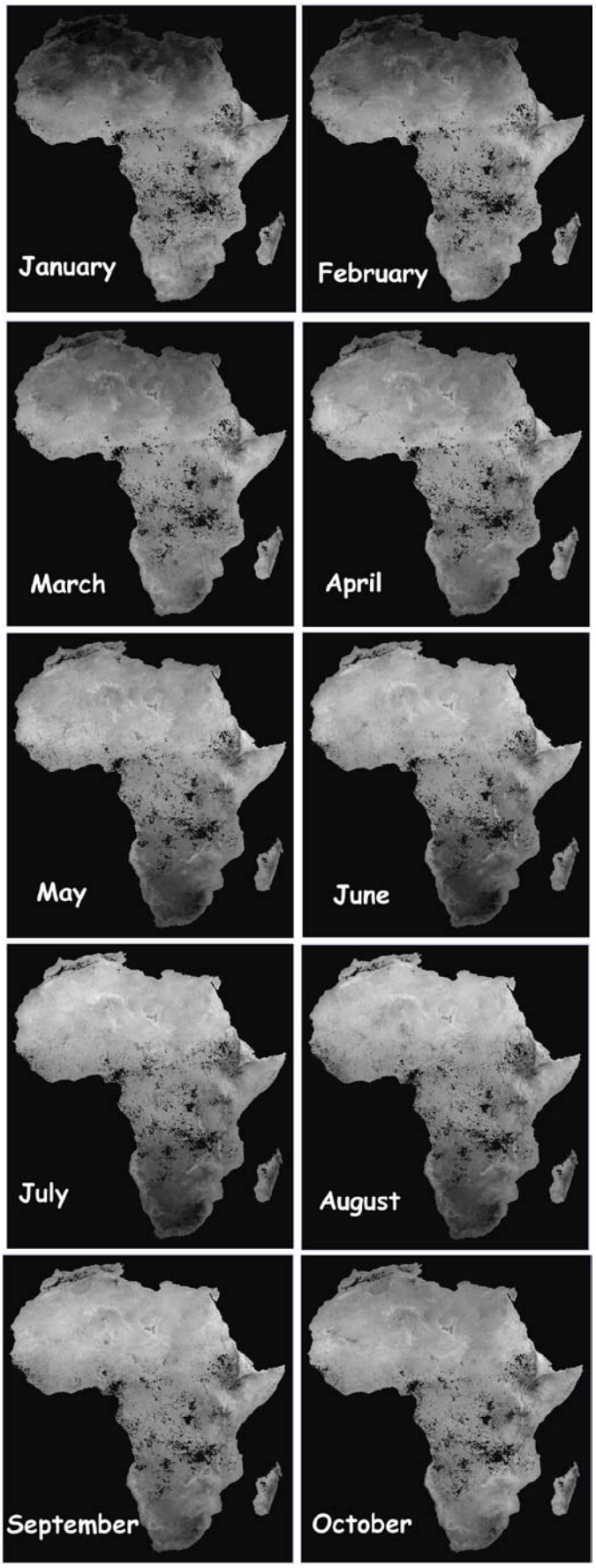


Fig. 2. The monthly night LST images (the lighter a pixel is the greater the LST). LST pixel values are in the range -2 to 38 degrees Celsius.

C. Tuberculosis Incidence Rates

TB according to the World Health Organization is now the world's leading killer of adults; 30 million adults are expected to die from TB in the next 10 years [16]. With the spread of HIV, coupled with deterioration of conditions in many cities, not just in developing countries, but throughout the developed world as well, and the explosion in international travel, a resurgence of TB has occurred [18].

The number of incidents per African country was downloaded from the World Health Organization database for the year 2008 [16]. The TB data standardized to incidence rates (IR) (number of incidents per 100,000 inhabitants) as well as the population per country are presented in Table I.

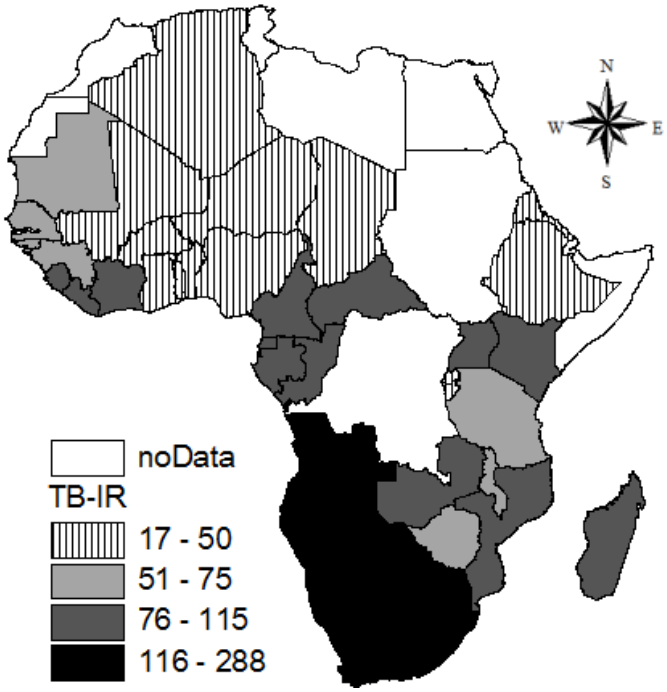


Fig. 03. The countries are categorized to 4 groups on the basis of TB-IR value (Table I).

TABLE I
POPULATION AND TB INCIDENCE RATES (IR) PER 100,000 INHABITANTS PER COUNTRY [16].

African countries	**Population**	**TB IR per 100,000**
Algeria	33,351,000	25.92
Angola	16,557,000	136.27
Benin	8,760,000	33.86
Botswana	1,858,000	180.36
Burkina	14,359,000	19.19
Burundi	8,173,000	44.17
Cameroon	18,175,000	78.31
Central African Republic	4,265,000	99.23
Chad	10,468,000	31.61
Congo	3,689,000	91.38
Cote D'Ivoire	60,644,000	114.57
Equatorial Guinea	496,000	109.07
Eritrea	4,692,000	17.88
Ethiopia	81,021,000	50.35
Gabon	1,311,000	114.57
Ghana	23,008,000	34.35
Guinea	9,181,000	71.46
Guinea-Bissau	1,646,000	74.30
Kenya	36,553,000	100.71
Lesotho	1,995,000	193.58
Liberia	3,579,000	84.88
Madagascar	19,159,000	80.33
Malawi	13,571,000	56.20
African countries	**Population**	**TB IR per 100,000**
Mali	11,968,000	39.56
Mauritania	3,044,000	52.73
Mozambique	20,971,000	89.76
Namibia	2,047,000	235.86
Niger	13,737,000	42.61
Nigeria	144,720,000	31.80
Rwanda	9,464,000	44.09
Senegal	12,072,000	62.82
Sierra Leone	5,743,000	101.45
South Africa	48,282,000	287.48
Swaziland	1,134,000	273.81
Tanzania	39,459,000	61.26
Togo	6,410,000	34.85
Uganda	29,899,000	76.14
Zambia	11,696,000	112.95
Zimbabwe	13,228,000	74.31

D. Terrain Segmentation from Multi-Temporal LST Data

K-Means cluster analysis was used in order to partition the 12-dimensional imagery into K exclusive clusters. It begins by initializing cluster centroids, then assigns each pixel to the cluster whose centroid is nearest, updates the cluster centroids, then repeats the process until the stopping criteria are satisfied [19]. It uses Euclidian distance for calculating the distances between pixels and cluster centroids. The underling idea of cluster analysis is that the cluster centroids represent the mean expression of the derived clusters.

The 12 thermal images (Fig. 2) presented a common arithmetic range of values in the interval [-2, 39] degrees Celsius and there is no need for data standardization [20]. In the current implementation of the method, small clusters with area extent (occurrence) less than 0.5% were eliminated by merging them with larger clusters that are closest to their centroids, while the stopping criterion was defined as the percentage of the migrating pixels during a specific iteration (if it was less than 0.1% of the entire image pixels the clustering was terminated). Eight clusters were mapped after 84 iterations. The cluster centroids (Table II) are presented in Fig. 4a and 4b.while their spatial distribution of the 9 cluster is given in Fig.5a.

TABLE III
THE CENTROID PER CLUSTER (FIG.2) AND THE CORRESPONDING OVERALL OCCURRENCE DEFINED AS PERCENT AREA OCCUPIED BY EACH CLUSTER (FIG. 4A).

Month	**Cluster Centroid (degrees Celsius)**								
	1	**2**	**3**	**4**	**5**	**6**	**7**	**8**	**9**
January	5.0	2.8	22.1	20.1	20.9	15.3	17.8	17.3	10.5
February	8.7	5.3	23.7	19.6	21.7	15.2	19.7	18.0	14.0
March	13.6	9.8	24.5	18.2	21.3	13.6	22.0	17.6	17.3
April	17.7	13.6	25.3	16.2	21.3	12.0	24.6	17.2	21.4
May	22.0	17.6	24.9	11.5	19.8	8.2	26.9	16.4	24.6
June	25.0	20.6	23.8	9.7	19.4	7.1	26.8	15.8	26.7
July	27.1	23.6	22.4	9.6	18.4	6.9	26.9	15.1	27.9
August	27.5	23.8	21.9	10.9	18.7	7.9	25.9	15.8	27.3
September	24.4	19.7	22.6	14.6	19.4	10.4	26.6	16.8	26.4
October	19.7	16.5	22.9	17.8	20.6	12.0	25.7	17.2	23.0
November	12.0	9.7	20.8	19.0	20.0	13.5	20.3	15.4	15.5
December	6.7	4.9	19.7	20.2	19.4	14.5	16.5	15.0	10.8
Occurrence %	13.0	5.0	14.5	9.9	20.1	4.8	10.4	9.2	13.0

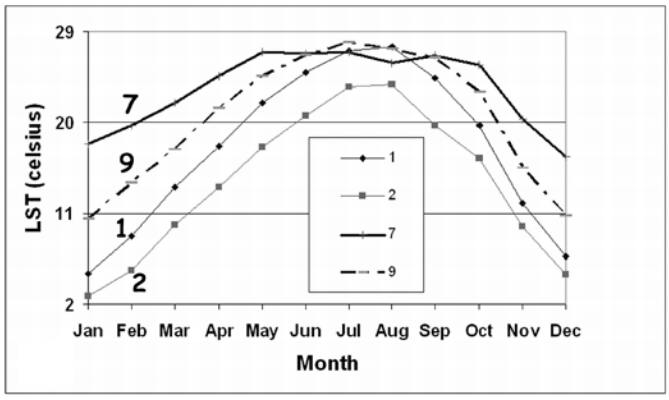


Fig. 4a. The 9 cluster centroids presented as mean LST per month curves. In order to assist interpretation the centroids of clusters 1, 2, 7 and 9 are presented separately here.

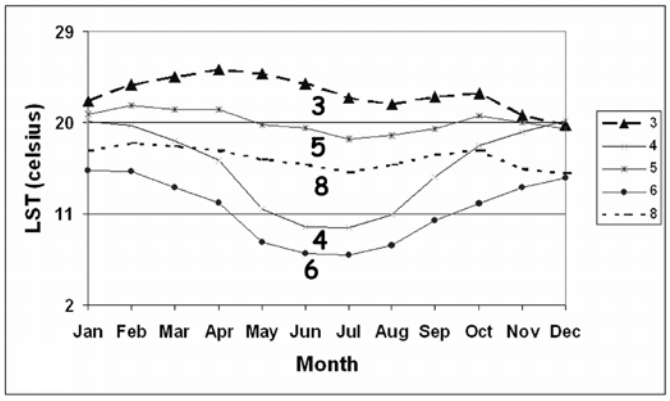


Fig. 4b. Representation of clusters 3, 4, 5, 6 and 8.

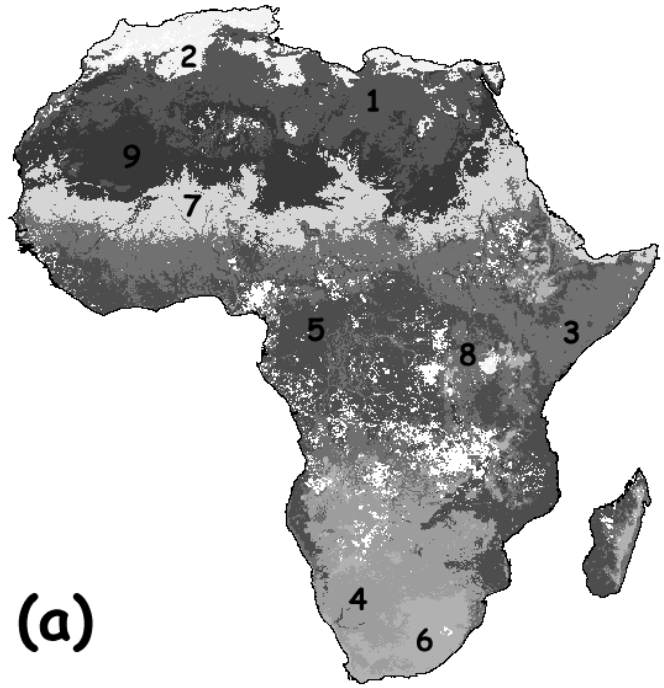


Fig. 5a. The spatial distribution of the 9 clusters derived by the segmentation of the 12 monthly night LST imagery

E. LST Representation of Spatial Objects

Countries form polygons (Fig. 1). Each polygon is projected to the cluster image (Fig. 5a). Then the percent of area (occurrence) occupied by each cluster per country is computed (Table III). Finally K-Means cluster analysis is applied to the parametric representation of countries (Table III) and 5 groups of country objects are defined (Fig. 5b).

TABLE IIIII
CLUSTER OCCURRENCE DEFINED AS PERCENT AREA PER COUNTRY OCCUPIED BY EACH OF THE 9 CLUSTERS (FIG. 4A). THE CLUSTERS (COLUMNS) WERE RANKED (2, 1, 9, 7, 3, 5, 8, 4, 6) ACCORDING TO THEIR SPATIAL DISTRIBUTION (IN A NORTH TO SOUTH DIRECTION). FOR THE COUNTRIES LABELED WITH THE ASTERISK (*) THERE ARE NO TUBERCULOSIS DATA IN WHO DATABASE (TABLE I).

Country	**Cluster occurrence (%) per country.**								
	2	**1**	**9**	**7**	**3**	**5**	**8**	**4**	**6**
Algeria	21.3	51.7	26.1	0.87					
Angola					0.3	17.1	38.3	37.5	6.6
Benin				0.05	86.3	13.6		0.0	
Botswana						1.2	1.0	91.6	6.3
Burkina				36.0	63.0	1.0			
Burundi	6.9		0.4			3.0	81.6		8.2
Cameroon				1.1	13.7	61.0	19.6	3.4	1.2
Central African Republic				0.19	23.0	72.0	4.8		
Chad	0.8	4.3	22.5	38.5	29.7	3.6	0.6		
Cote D'Ivoire					44.4	54.0	0.64	0.9	
Dem. Rep. Of Gongo*	1.6	0.3	0.5		5.7	64.2	25.3	1.3	1.0
Djibouti*				76.9	23.1				
Egypt*	15.5	57.9	20.4	6.2					
Equatorial Guinea						51.1	35.5	3.0	10.4
Eritrea			0.2	42.8	41.8	9.8	5.4		0.1
Ethiopia				4.1	33.7	22.9	25.2	0.9	13.2
Gabon	0.3				1.4	81.7	16.4	0.1	0.1
Ghana					54.9	44.9		0.08	
Guinea					32.6	60.1	6.4	0.8	
Guinea-Bissau				7.9	49.5	37.9	2.4	2.2	
Kenya	0.1				57.6	19.5	15.3	0.1	7.3
Lesotho									100
Liberia						88.5	4.4	6.9	0.1
Libya*	15.2	73.2	11.5	0.1					
Madagascar			0.3		3.6	49.1	28.4	3.9	14.7
Malawi	2.0	2.6	4.1			24.7	45.1	19.9	1.6

Country	Cluster occurrence (%) per country.								
	2	**1**	**9**	**7**	**3**	**5**	**8**	**4**	**6**
Mali	0.05	0.8	43.0	38.6	15.1	2.2	0.3		
Mauritania	0.4	14.7	58.0	26.4	0.2	0.3	0.1		
Morocco*	62.5	20.7	12.5				4.3		
Mozambique		0.2	0.2		1.3	76.3	10.2	11.7	0.1
Namibia					0.3	9.9	7.6	69.2	13.0
Niger		3.3	48.9	40.4	5.2	1.9	0.2		
Nigeria			1.6	15.4	45.5	32.0	2.3	3.1	0.1
Rep. Of Congo	0.1				12.5	77.4	10.0		
Rwanda	0.9					0.4	73.6		25.2
Senegal			0.2	39.4	46.2	14.0	0.3		
Sierra Leone					1.1	80.2	4.8	13.9	
Somalia*			0.1	13.4	76.0	8.9	1.5		
South Africa						1.2	2.4	37.9	58.5
Sudan*		4.9	19.3	29.2	35.9	9.8	0.6	0.3	0.01
Swaziland						4.5	36.2	42.4	16.9
Tanzania	1.9	0.5	0.5		0.6	48.8	42.6	1.1	4.0
Gambia*				14.5	51.3	33.9		0.3	
Togo					66.4	33.6			
Tunisia*	70.6	27.3	2.1						
Uganda	3.5				0.8	36.7	54.2	0.2	4.7
Western Sahara*	6.6	29.7	46.7	0.5		0.3	16.1		
Zambia	1.0	0.02	0.1		0.14	15.5	27.4	55.2	0.6
Zimbabwe			0.1	0.1		21.7	2.5	72.3	3.2

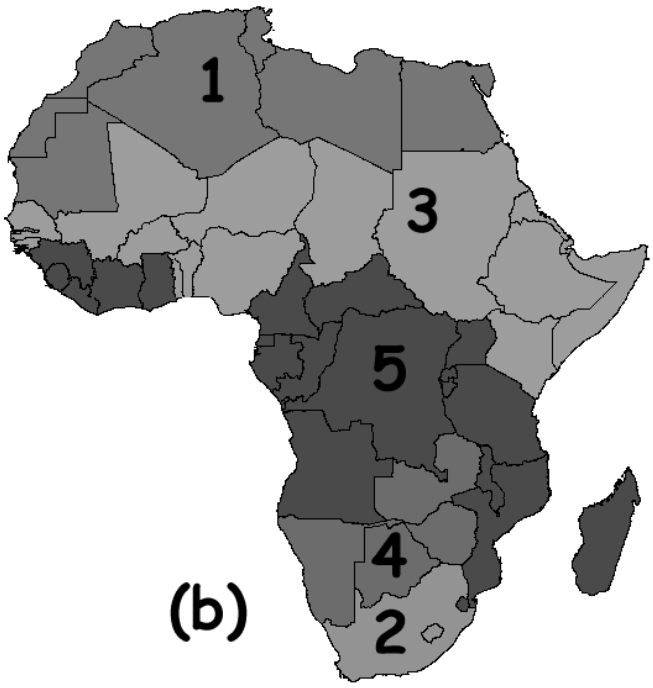


Fig. 5b. The 5 groups of African countries derived by K-Means cluster analysis applied to the objects parametric representation scheme presented in Table III.

F. TB IR correlation to climatic zones occurrence per country

Figure 6 indicates that there is an increase of TB-IR per country if the percent occurrence of either zone 4 or zone 6 is increased. This relationship appears to be stronger for zone 4.

The correlation coefficient (r) between the percent area of zone 4 and the TB-IR per country equals to 0.589. The relationship between the correlated attributes will be further explored by assuming a linear regression model given in below equation indicating that,

$$\text{Percent of Zone 4} = 76.72 + (1.523^{*}\ \text{TB-IR}) \quad \text{(Equation.1)}$$

The test statistics for the significance of the regression model is distributed as the variance ratio (F) between the regression variance to residual variance [22]. The null hypothesis under the test is that of no explanation of the variability of TB-IR in terms of percent of zone 4.

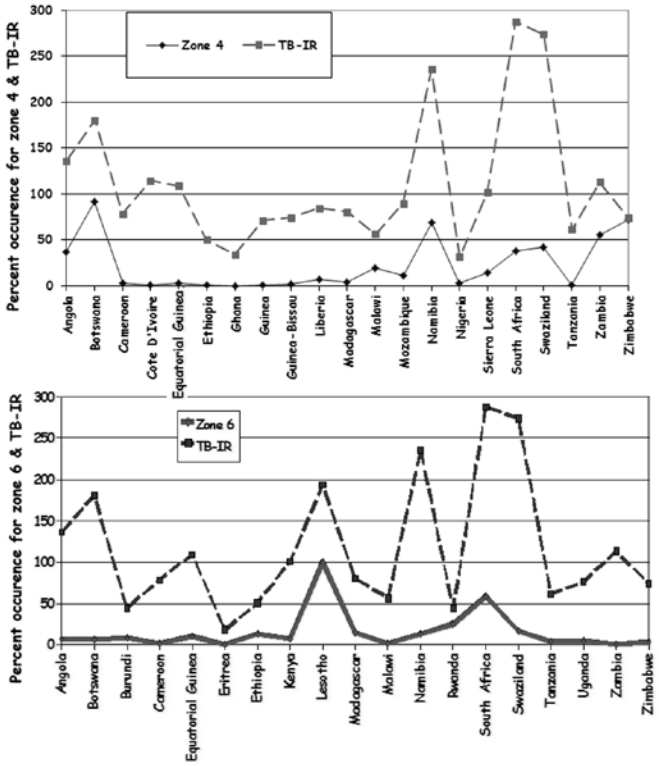


Fig. 06. TB-IR per country (Table I) is increased with the percent of the area occupied by the zones 4 and 6 (Table III, Figure 3).

The computed variance ratio for the equation 1 equals to 10.068 (Table IV).

TABLE IVV

ANALYSIS OF VARIATION (ANOVA) FOR THE LINEAR REGRESSION OF TB-IR VERSUS PERCENT OF ZONE 4 PER COUNTRY (EQUATION 1).

ANOVA	df	SS	MS	F
Regression	1	37235.82	37235.82	10.06871
Residual	19	70265.25	3698171	
Total	20	107501.1		

The variance ratio is far greater than the tabled F critical value at 0.01 significance level for (1, 19) degrees of freedom and the null hypothesis is rejected. Figure 7 also proves graphically the linear correlation between the variables, although some outliers exist.

Figure 8 identifies that the countries with maximized TB-IR value (TB-IR>110) according to Table I also present maximized percent occurrence of zone 4 (Table III) and are spatially distributed in the southwest Africa.

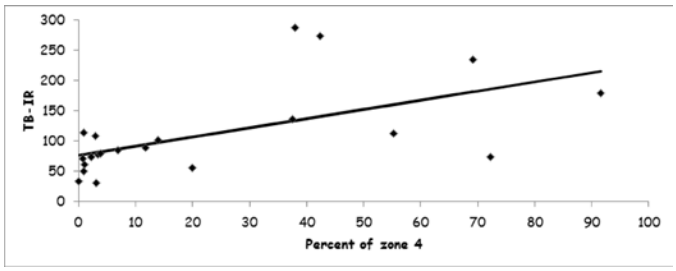


Fig. 07. The linear regression of TB-IR versus the percent occurrence of zone 4 per country.

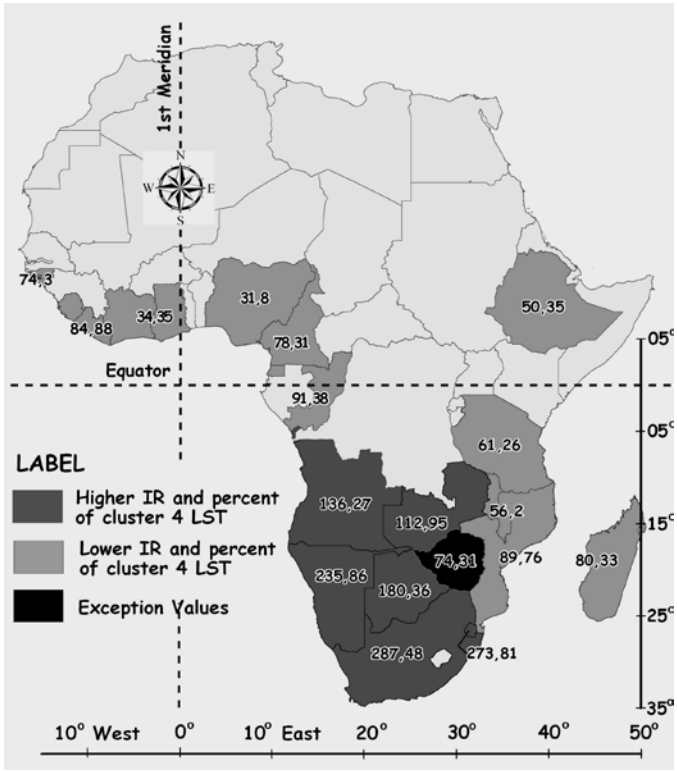


Fig. 08. The countries in dark grey are formed by objects with both increased TB-IR value (TB-IR>110 - Table I) and percent occurrence of zone 4 (Table III) while the countries in light grey present intermediate TB-IR value and percent occurrence of zone 4 per country that is lower than the percent occurrence of zone 6 (Table III). Zimbabwe is exception since the percent occurrence of zone 6 per country is lower than the percent occurrence of zone 4.

The southeast African countries, across the Indian Ocean, present intermediate TB-IR values while the percent occurrence of zone 4 per country is lower than the percent occurrence of zone 6 (Table III). Zimbabwe is an exception (Figures 1 and 8) since the percent occurrence of zone 6 per country is lower than the percent occurrence of zone 4.

III. DISCUSSION OF THE RESULTS

The interpretation of thermal terrain segmentation (both the spatial distribution of clusters in Fig. 5a and the cluster centroids in Table II and Figures 4a and 4b) reveal the seasonal differences observed in between the northern and southern hemisphere and map in an objective way the borders of the identified zones. The centroid LST curves for clusters 1, 2, 7 and 9 correspond to typical northern hemisphere curves (with maximum LST observed during the summer period while minimum LST is evident during the winter). The centroid curves are ranked in increasing LST order from 2 to 1, 9 and 7 (Fig. 4a). Figures 4a and 4b indicate that the warmer the LST centroid-co-ordinates are, the southern the cluster's spatial distribution is.

On the contrary, the clusters 4 and 6 are spatially distributed in southern part of the continent (Fig. 4b) and present centroid curves that are typical of the southern hemisphere (maximum LST values are observed during the winter period, while minimum LST values are observed during the summer). The centroid curves (Fig. 4b) of clusters 3, 5 and 8 (spatially distributed in the central part of Africa), present maximum centroid co-ordinates in both the spring and the autumn season while the relative LST differences between the various seasons are minimum. This pattern corresponds rather to the tropical climatic zone.

Thus, thermal terrain segmentation from multi-temporal monthly night imagery, outline in an objective way both the temporal variation of LST during the 2008 as well as the spatial distribution of climatic zones.

Table III, contains the LST signature for each African country. The LST signature actually reveals the percent of the country occupied by the regions

belonging to each of the 9 clusters defined in Fig. 5a. The K means cluster analysis applied to the LST countries signature (Table III), and grouped countries to 5 groups with almost similar LST signatures. The Cluster 1 is formed by the northern African countries, (Egypt, Libya, etc.), while cluster 2 corresponds to South Africa. The clusters 3, 4 and 5 are spatially distributed in between clusters 1 and 2 (Fig. 5b). This information is of particular interest in planning, environmental assessment and climatic change studies since it indicates the balance of the various regional LST zones that are evident within each country.

On the other hand a correlation was established among TB-IR and specific climatic zones as they were defined from the LST clustering. Such evidence was already known, but it is the first time that this correlation was quantified on the basis of high resolution LST data comparable to the previous studies that were based on the very sparse meteorological stations network.

TB-IR values are maximized for the southern hemisphere and they are correlated to the occurrence of the climatic zone with LST signature corresponding to clusters 4 and 6. These clusters present an annual variation of LST that is typical of the southern hemisphere while cluster 6 is colder that cluster 4 (Fig. 3b). TB-IR values are maximized for the southern and western African countries with maximized occurrence of cluster 4. It seems that there is a correlation in between TB-IR values and LST annual variation although additional biophysical and socioeconomic factors should be taken into account.

IV. Conclusions

In this study the biophysical data was expressed at a country level for statistical evaluations to be feasible, since TB-IR data are available per country [16].

The thermal terrain segmentation was achieved on the basis of MODIS monthly averaged LST from the night (10:30 PM) passes that are available from the Terra satellite. Note that noon (1:30 AM) and night (1:30 PM) passes are also available daily from the Aqua satellite that also carries a MODIS instrument. These datasets are available since 2001 and so monthly variations of LST four times (10:30 AM, 1:30 AM, 10:30 PM, 1:30 PM) per day might be studied and correlated to vegetation, agriculture, and land cover studies at moderate resolution scale.

Thermal terrain segmentation from multi-temporal monthly night imagery, outline in an objective way both the temporal variation of LST during the 2008 as well as the spatial distribution of LST zones. The country LST signatures derived for 2008 are a tool for environmental comparisons between different countries while clustering grouped African countries to subsets presenting similar night monthly LST variation. On the other hand the LST signatures were correlated to TB-IR values. Modern biophysical imagery will play a key role in the monitoring of both the climatic zones and TB-IR values variation that are of particular interest due to the upcoming climatic change.

Acknowledgments

The authors acknowledge to the anonymous reviewers for their important comments.

References

[1] E. Bartholome, and A.S. Belward, CLC2000, a new approach to global land cover mapping from Earth observation data. Int. J. of Remote Sensing, vol. 26, p.p. 1959-1977, 2005.

[2] T. Lillesand, R. Kiefer and J. Chipman, Remote Sensing and Image Interpretation (6th edition). John Wiley & Sons, New York, p. 763, 2008.

[3] J.E. Vogelmann, T.L. Sohl, P.V. Campbell and D.M. Shaw, Regional Land Cover Characterization Using Landsat Thematic Mapper Data and Ancillary Data Sources. Environmental Monitoring and Assessment, vol. 51, p.p. 415-428, 1998.

[4] G. Miliaresis, The Landcover Impact to the Accuracy of the SRTM-1 Finished Dataset. Sensors, vol. 8, p.p. 3134-3149, 2009.

[5] G. Miliaresis, The terrain signatures of administrative units: a tool for environmental assessment. Environmental Monitoring & Assessment, vol.150, p.p. 386-396, 2009.

[6] Z. Wan, Y. Zhang, Q. Zhang and Z.L. Li, Quality assessment and validation of the MODIS land surface temperature. Int. J. of Remote Sensing, vol. 25, p.p. 261-274, 2004.

[7] G. Miliaresis, Regional thermal and terrain modeling of the Afar Depression from multi-temporal night LST data. Int. J. of Remote Sensing, vol. 30(9), p.p. 2429–2446, 2009.

[8] G. Miliaresis and K. S. Seymour, 2010, Mapping the spatial & temporal SST variations in Red Sea, revealing a probable regional geothermal anomaly from Pathfinder V5 data. Int. J. of Remote Sensing, 18 pages, DOI: 10.1080/01431161003631568.

[9] G. Miliaresis and A. Tsatsaris, Thermal terrain modeling of spatial objects, a tool for environmental and climatic change assessment. Environmental Monitoring & Assessment, vol. 164, p.p. 561-572, 2010.

[10] A. Tsatsaris, P. Iliopoulou, A. Panagiotopoulou and Y. Tselentis, "A Geographical Database for the Control of Leishmaniasis: The Case of Greater Athens, Greece". In Proc. 10th International Symposium on Health Information Management Research, 2005, Thessalonica, Greece, paper 10, p.120.

[11] P.R. Epstein, Climate change and emerging infectious diseases. Microbes and Infection, vol. 3, p.p. 747–754, 2001.

[12] N. Naranbat, P. Nymadawa, K. Schopfer, and H. L. Rieder, Seasonality of tuberculosis in an Eastern-Asian country with an extreme continental climate. European Respiratory Journal, Vol.34, p.p. 921-925, 2009.

[13] B. Mabaera, N. Naranbat, A. Katamba, D. Laticevschi, J. M. Lauritsen and H. L. Rieder. Seasonal variation among tuberculosis suspects in four countries. International Health, vol. 1, p.p.53-60, 2009.
[14] Schlouter, T, Geological Atlas of Africa. Springer, Berlin Heidelberg, p. 272, 2006
[15] WIST, (2008). Data interface. NASA/GSFC, Greenbelt, MD, [Online] Available: https://wist.echo.nasa.gov/api
[16] WHO, (2010). Global Tuberculosis Database. The World Health Organisation. [Online] Available: http://apps.who.int/globalatlas/dataQuery/default.asp
[17] African Maps, (2010). Political map of Africa. Perry-Castañeda Library Map Collection. The University of Texas, Austin, [Online] Available: http://www.lib.utexas.edu/maps/africa.html
[18] R. R. Colwell, Global Climate and Infectious Disease: The Cholera Paradigm, Science, New Series, Vol. 274, No. 5295, p.p. 2025-2031, 1996
[19] P. Mather, Computer Processing of Remotely- Sensed Images (3rd edition). John Wiley and Sons, New York, p. 292, 2004
[20] G. Miliaresis and P. Illiopoulou, Clustering of Zagros Ranges from the Globe DEM representation. Int. Journal of Applied Earth Observation & GeoInformation, vol. 5, p.p. 17-28, 2004.
[21] G. Miliaresis, Quantification of Terrain Processes. Lecture Notes in Geoinformation & Chartography, vol. XIV, p.p. 13-28, 2008.
[22] G. Shaw and D. Wheeler, Statistical techniques in geographical analysis. John Wiley & Sons, Chichester, 364 p., 1985.